Comparison of Distributional Statistics of *Aquarius* and Argo Sea Surface Salinity Measurements

ELIZABETH MANNSHARDT, KATARINA SUCIC, AND MONTSERRAT FUENTES

Department of Statistics, North Carolina State University, Raleigh, North Carolina

FREDERICK M. BINGHAM

Center for Marine Science, University of North Carolina at Wilmington, Wilmington, North Carolina

(Manuscript received 16 April 2015, in final form 5 October 2015)

ABSTRACT

Salinity is an indicator of the interaction between ocean circulation and the global water cycle, which in turn affects the regulation of the earth's climate. To thoroughly understand sea surface salinity's connection to processes that define the hydrological cycle, such as surface forcing and ocean mixing, there is need for proper validation of remotely sensed salinity products with independent measurements, beyond central tendencies, across the entire distribution of salinity. Because of its fine spatial and temporal coverage, *Aquarius* presents an ideal measurement system for fully characterizing the distribution and properties of sea surface salinity. Using the first 33 months of *Aquarius*, version 3.0, level 2 sea surface salinity data, both central tendencies and distributional quantile characteristics across time and space are investigated, and a statistical validation of *Aquarius* measurements with Argo in situ observations is conducted. Several aspects are considered, including regional characteristics and temporal agreement, as well as seasonal differences by ocean basin and hemisphere. Regional studies examine the time and space scales of variability through time series comparisons and an analysis of quantile properties. Results indicate that there are significant differences between the tails of their respective distributions, especially the lower tail. The *Aquarius* data show longer, fatter lower tails, indicating higher probability to sample low-salinity events. There is also evidence of differences in measurement variation between *Aquarius* and Argo. These results are seen across seasons, ocean basins, hemispheres, and regions.

1. Introduction

In 2011, NASA launched a satellite mission to measure sea surface salinity (SSS) and to provide the global view of salinity variability needed for climate studies. The goal of the *Aquarius* mission is to understand "the interaction between ocean circulation, the water cycle, and climate by measuring salinity" (NASA 2012). Salinity affects the interaction between ocean circulation and the global water cycle, which in turn affects the regulation of the earth's climate through the ocean's capacity to store and transport heat and affects the onset of phenomena such as El Niño (Lagerloef et al. 2008). Characterizing salinity is vital to understanding the interaction between ocean circulation, the water cycle, and climate. Given a properly validated salinity product, *Aquarius* provides a spatially rich source of information about ocean salinity in a time frame that allows for the consideration of mesoscale regional events as well as global climate fluctuations.

The core of the *Aquarius* mission is the retrieval algorithm, the process by which satellite-measured microwave brightness temperatures are transformed into values of SSS. This complex algorithm has been well documented (Le Vine et al. 2007; Yueh and Chaubell 2012; PO.DAAC 2014) and is based on the dielectric model of Klein and Swift (1977). Some of the major issues with the retrieval algorithm have been radio frequency interference and the reflection of cosmic background radiation off a rough sea surface (Lagerloef et al. 2013; Meissner et al. 2014a). Validation, the comparison of retrieved values of SSS with values measured by in situ instrumentation, feeds

Corresponding author address: Elizabeth Mannshardt, Department of Statistics, North Carolina State University, 2311 Stinson Dr., Raleigh, NC 27695-8203.
E-mail: mannshardt@stat.ncsu.edu

DOI: 10.1175/JTECH-D-15-0068.1

back into the retrieval algorithm to update and improve the algorithm. Over the life of the mission, the retrieval algorithm has undergone a number of upgrades and improvements based on the results of validation studies.

One of the main goals behind the launch of *Aquarius* was the idea of using it as an ocean rain gauge (Lagerloef et al. 2008; Yu 2011), whereby changes in surface salinity would be used to infer changes in freshwater flux across the surface. As the mission has progressed, however, this goal has become more problematic as researchers have come to understand how important ocean dynamics are in determining the field of SSS (Yu 2014, 2010; Alory et al. 2012; Foltz and McPhaden 2008; Lee et al. 2012; Qu et al. 2011; Vinogradova and Ponte 2013; among others). There is not a direct relationship between freshwater flux and changes in SSS.

One of the most difficult aspects in the validation of *Aquarius* is the comparison of the satellite data to the existing in situ data, particularly Argo floats. Since the floats typically turn their sensors off at 3–5-m depth, and the satellite measures a near-surface (1–10 cm) value, the two measurements are not necessarily comparable. This is thought to result in *Aquarius* being biased low relative to Argo in regions with large rainfall like the intertropical convergence zone (ITCZ) and South Pacific convergence zone (SPCZ) (Tang et al. 2014a). Low-salinity events associated with rainfall are often confined to the near surface. In this context, near surface means the upper 1–2 m. Various authors have found that in the short term, the salinity impacts of rain events do not usually penetrate much farther than this (Henocq et al. 2010; Boutin et al. 2014, 2013; Santos-Garcia et al. 2014; Tang et al. 2013, 2014b; Asher et al. 2014b). Some progress is being made in this area, however, as we come to more effectively incorporate wind speed into the retrieval algorithm (Meissner et al. 2014a) and quantify the impact of rainfall on the float data (Drucker and Riser 2014).

As suggested by Drucker and Riser (2014), perhaps one possible way to return to the idea of the ocean rain gauge is to examine the differences between Argo and *Aquarius* when there is rainfall that freshens the surface. In this situation, it is important to know how the *Aquarius* instrument is performing for values of SSS that are low compared to the background value. In other words, we need to quantify the lower tail of the SSS distribution. Perhaps by understanding these differences, we can better use the *Aquarius* data to serve one of the original purposes of the mission. Thus, there is a need to examine not just the mean or median values of SSS from *Aquarius*, but the entire distribution to ensure that low SSS events in particular are being well measured.

Now that the basic product has approached a level of accuracy that makes it useful for science, a more nuanced view of the validity of the data is required, one that seeks to ensure the accuracy across the entire distribution of SSS. SSS tends to have a probability distribution that is skewed toward lower salinity values (Bingham et al. 2002) and often has an upper limit in a particular area, above which SSS is rarely observed. A plausible explanation of this has to do with rainfall, which adds freshwater to the surface ocean, making it stably stratified. Rain events freshen the water for time periods lasting from hours to days (Boutin et al. 2013; Henocq et al. 2010; Asher et al. 2014a). By contrast, the processes that make the surface ocean saltier, mainly evaporation, also make the water column unstable and overturn quickly (Hodges and Fratantoni 2014; Asher et al. 2014b; Yu 2010). Advection can also play a significant role in generating anomalies at both the upper and lower ends of the distribution (e.g., Busecke et al. 2014; Hasson et al. 2014).

The main dataset used to validate *Aquarius* is Argo floats (Argo 2000). Before the Argo era, it was barely possible to determine a mean, much less try to understand the variability or any extreme values over much of the ocean (Bingham et al. 2002). The new *Aquarius* dataset has given us the ability to characterize the probability of extreme values of SSS (OBPG 2014). What has not been done is the necessary step of comparing the probability distributions of the Argo and *Aquarius* datasets to determine whether they come from populations with similar characteristics.

Each salinity product has its advantages and limitations. We use an *Aquarius*, version 3.0 (V3.0), level 2 data product based on radiation input and deterministic relationships that provides complete global spatial coverage over 7 days. Argo is temporally complete on a 10-day scale but is spatially sparse globally. In addition, there are several sources of uncertainty in *Aquarius* measurements. The error budget for *Aquarius* measurements are briefly described in section 2b and further detailed in Lagerloef et al. (2008, 2013). Errors likely exhibit long correlation scales over time, and the error budget allocated for each source of error varies with latitude. There are additional considerations as a result of the retrieval algorithm, including processing biases resulting from contamination by other signals. To fully understand and characterize these processing errors and biases could involve characterization of the *Aquarius* signal under different versions of the *Aquarius* data processed in different ways [rain corrected versus not, combined active–passive (CAP) versus non-CAP, V4.0

versus V3.0, etc.]. This is beyond the scope of this manuscript, but it would be an important extension to the work presented here.

Argo floats and *Aquarius* measure different quantities. Argo measures bulk surface salinity (top 10 m), whereas *Aquarius* measures skin values (top 1–10 cm). The distinction between bulk and skin values of SSS is an active area of research (Henocq et al. 2010; Boutin et al. 2014; 2013; Santos-Garcia et al. 2014; Tang et al. 2013, 2014b). Most previous *Aquarius* validation analyses have treated these datasets as directly comparable (Lagerloef et al. 2013; Tang et al. 2014a; Abe and Ebuchi 2014). There are additional considerations due to the retrieval algorithm, including processing biases as a result of contamination by other signals. Fully understanding the difference between the two products is a matter of not only doing a direct point-by-point comparison but deconvolving that comparison from the very different sampling schemes, and the space and time scales inherent in the SSS field itself.

We consider sea surface salinity between 30°S and 30°N latitude from 25 August 2011 to 1 June 2014 to conduct an initial exploration of the physical validation of *Aquarius* measurements with Argo observations. Diagnostics are compared to calibrate the spatial and temporal agreement of *Aquarius* and the well-utilized in situ Argo float data. We also considered spatial characteristics and temporal agreement, as well as regional differences by ocean basin and hemisphere. Results are in general agreement with the *Aquarius* salinity validation analysis (Lagerloef et al. 2013) produced by the *Aquarius* Science Team based on the V2.0 data. However, we go beyond this by considering the entire probability distribution, especially the lower tails.

Section 2 describes the *Aquarius* and Argo data used in this paper. It is important to consider the distributional characteristics of salinity across time and space in order to facilitate a full understanding of the complex interactions across the hydrological cycle and global transport of freshwater. Section 3 considers a validation of the distributional characteristics of *Aquarius* measurements performed with Argo in situ observations, including a seasonal study by hemisphere and ocean basin by means of a comparison of Argo and *Aquarius* via observations matched across time and space. Section 4 details the temporal trends across eight regions defined within the 30°S and 30°N area of study in order to better describe the differences in seasonal and regional trends. Section 5 considers a comparison of *Aquarius* and Argo between a dry region and a rainy region. The Salinity Processes in the Upper Ocean Regional Study 1 and 2 (SPURS-1 and SPURS-2, respectively) regions are examined because of both their oceanic and meteorological properties, in order to begin to understand separating the effects of ocean dynamics from local meteorology, as well as because of their general scientific interest. Finally, section 6 provides a discussion of the findings and the important characteristics of salinity for which this paper offers a fuller description.

2. Data

This section details the sources and data processing techniques for the data utilized in this paper.

a. Aquarius data

The *Aquarius* data used in this paper are the level 2 swath-based data from version 3.0 (OBPG 2014). Files were downloaded from the PO.DAAC *Aquarius* data archive (http://podaac.jpl.nasa.gov). Data quality for *Aquarius* decreases rapidly poleward of the 30°S and 30°N latitudes, especially differences between ascending and descending passes (Lagerloef et al. 2013). Therefore, for this study we used only data between 30°S and 30°N, binned and averaged to ½° along-track intervals between those latitudes.

The satellite has a 7-day repeat track of 103 orbits or about 15 orbits per day (PO.DAAC 2014). Each orbit has three beams. The final dataset presented here consists of about 144 repeat cycles, each 1 week long, the first 33 months of available *Aquarius* data, spanning the time period from 25 August 2011 to 1 June 2014. The array generated had salinity values indexed by beam, orbit, ascending/descending state, and latitude/longitude. Each of the orbits defines a set of locations identified by beam number (three beams), repeat track, ascending/descending (two states), and latitude/longitude (120 bins, centered every ½° at 29.75°S–29.75°N). For clarity, we call each of these ($3 \times 144 \times 2 \times 120 = 103\,680$) points a node. Each node represents an SSS measurement with a footprint of about 100 km in diameter (PO.DAAC 2014).

The level 2 data were used rather than level 3 gridded data in order to avoid extraneous smoothing tying adjacent nodes to each other, and thus each node time series becomes an independent set of measurements. The initial quality control performed on the *Aquarius* salinity data for this paper was a gross range check, a check for land proximity, deletion of obviously erroneous values, and a check for valid orbital position. Data with a land fraction greater than ½% were removed to avoid spurious measurements due to land surface interaction. Measurements of salinity above 40 or below 20 psu were considered spurious for this analysis and were removed. This minimal truncation removed 85 of

the total 3 681 718 available *Aquarius* measurements, less than 3/1000 of 1% of the total data.

b. *Uncertainty sources in* Aquarius *measurements*

There are several sources of uncertainty in *Aquarius* retrievals, including radiometer noise, antenna pointing error, surface roughness, ionospheric interference, galactic background reflection, and sea surface temperature uncertainty (Lagerloef et al. 2008). Using a triple-point analysis comparing satellite, in situ, and model values, Lagerloef et al. (2013) concluded that the 2.0 version of the *Aquarius* dataset has a global monthly root-mean-square (RMS) error of 0.3. Preliminary release version 2.7.1 has an RMS value between 0.22 and 0.3 (Tang et al. 2014a). Abe and Ebuchi (2014) compared the V3.0 standard, CAP, and Remote Sensing Systems (RSS) products with collocated Argo floats; they found RMS differences of 0.42, 0.51, and 0.41, respectively. The same calculation using the tropical moored buoy array yielded RMS differences of 0.35, 0.39 and 0.35, respectively.

As Lagerloef et al. (2013) indicate, many of the issues with regard to the quality of the *Aquarius* SSS product are exacerbated at higher latitudes and closer to coastal regions. We have taken care in this work to avoid such problems by confining the study to equatorward of 30° latitude and in areas away from the coast. Thus, we presume that the *Aquarius* accuracy for our study is better than the value of 0.3 quoted above, though we cannot say exactly what that value is. In addition, a source of uncertainty in *Aquarius* measurements includes the deterministic model input for the Hybrid Coordinate Ocean Model data product (PO.DAAC 2014) that is used as starting values in the algorithm for obtaining the *Aquarius* product.

The main continuing source of error is the reflection of cosmic background radiation from a nonsmooth ocean surface. This manifests itself in quasi-seasonal differences between ascending and descending passes, especially in the Southern Hemisphere. Ascending/descending path bias is much improved in version 3.0 over previous versions (Lagerloef et al. 2015). (Indeed much of the analyses detailed in this paper were performed separately on ascending and descending data with little difference found.) Thus, an ascending/descending path comparison is not a focus of the analyses considered in this paper. Other problems that are under active study are radio frequency interference (RFI) and antenna coupling issues that occur near the ITCZ. Again, however, this level of error is lower than for previous versions of the dataset. In particular, the radiometer calibrations are improving with time.

c. *Argo data*

We used Argo data (Argo 2000) spanning the time period 25 August 2011–1 June 2014. We used all available profiles in the 30°S–30°N range that had a data quality flag of good, taking the topmost salinity value above 10-m depth. Measurements of salinity above 40 or below 20 psu were considered spurious for this analysis and were removed. This truncation removed 417 of the 90 398 Argo measurements, less than one-half of 1% of the available measurements. SSS measurements from the Argo floats deployed during the SPURS mission in September of 2012 were removed for this validation analysis, so as not to bias overall SSS trends and comparisons with *Aquarius*. Twenty-four floats were deployed here, in the middle of the high salinity region of the subtropical North Atlantic, which sampled more frequently than other floats for some time. Thus, including the SPURS floats would increase the bias substantially. This masking removed 2381 Argo observations in the time period and region of study. An additional 785 observations were removed due to corresponding invalid pressure readings and/or possible individual float bias.

d. *Matching observations*

To determine the specific global agreement, *Aquarius* and Argo observations were matched on a 50-km footprint centered at the latitude and longitude by binned *Aquarius* measurement. *Aquarius* and Argo were then matched by calendar date to achieve maximum accuracy across possible mesoscale and microscale surface weather events. This results in $N =$ 41 544 matches across the entire time period and region between 30°N and 30°S latitude.

3. Distributional characteristics

In this section we consider a global comparison as well as a seasonal study by hemisphere and ocean basin. We study the distributional characteristics, including mean and variance, as well as noncentral tendency comparisions across distributional quantiles.

a. *Global comparison*

We compare the relative agreement of the global distribution of salinity across the entire time period. The global means differ slightly across the two matched products, with the *Aquarius* global mean equal to 34.93 and the Argo global mean value of 35.10. Note that these are different but comparable to the median (0.50 quantile) values of 34.97 for *Aquarius* and 35.11 for

TABLE 1. Global salinity quantiles: Argo and *Aquarius*. For example, the 0.10 quantile indicates the salinity for which 10% of observed values are less and 90% are greater.

Matched	*N*	0.01	0.05	0.10	0.25	0.50	0.75	0.90	0.95	0.99
Aquarius	41 544	32.74	33.47	33.81	34.32	34.97	35.48	36.02	36.44	37.43
Argo	41 544	33.18	33.86	34.13	34.55	35.11	35.56	36.13	36.54	37.42

Argo (Table 1). Additionally, 95% confidence intervals (CI) are calculated for the global means in which the standard deviations are calculated using a bootstrap method (Efron and Tibshirani 1986) to account for the high spatial and temporal dependency in the measurements for both products and the nonrandom sampling scheme inherent in the original data collection. A sensitivity analysis was run on the number of bootstrap replications with $R = 1000$ bootstrap iterations showing stable estimations. The standard deviations are 0.923 for *Aquarius* and 0.844 for Argo. This results in 95% confidence intervals for the global means of (34.877, 34.992) and (35.047, 35.151) for *Aquarius* and Argo, respectively. The confidence intervals for the mean global salinity products do not overlap, which indicates that the global means are significantly different across the two salinity products.

To compare the spread of measurements across *Aquarius* and Argo, confidence intervals for the standard deviations of each product were calculated utilizing the chi-square distribution according to Sheskin (2011). The standard deviations exhibit different properties, with 95% confidence intervals of (0.8861, 0.9692) and (0.8102, 0.8862) for *Aquarius* and Argo, respectively, with the Argo product showing slightly less global variation. This could indicate lower accuracy of individual *Aquarius* measurements or could indicate a fundamental difference in the skin versus depth measurement sampling. There is slight overlap in confidence intervals for the global standard deviations, indicating no significant difference in global variation between *Aquarius* and Argo.

The empirical densities of the matched Argo and *Aquarius* observations are in relative agreement (Fig. 1); however, Argo shows more fluctuations in the upper tail of the distribution and *Aquarius* shows a longer, slightly heavier lower tail. To more fully explore the entire SSS distribution, particularly in the tails, we consider an empirical quantile analysis (Table 1). The overall global quantiles for *Aquarius* and Argo show the same relative trends across the distributions: that is, *Aquarius* captures a slightly heavier lower tail. This is possibly due to the surface-level measurements afforded by *Aquarius*, whereas the Argo measurements may have a depth effect. For instance, *Aquarius* has lower 0.01 and 0.05 quantile values (32.74 and 33.47, respectively) than Argo (33.18 and 33.86, respectively), which indicates that *Aquarius* has a higher probability of observing low values than Argo. This is also seen at the 0.10 and 0.25 quantile levels. There is also evidence that there is much less of a tendency for the upper tails to differ. This can be seen in the upper quantile levels, where *Aquarius* has a 0.99 quantile value of 37.43 compared to Argo's corresponding value of 37.42.

To formally test whether the quantile levels across *Aquarius* and Argo are statistically different, confidence intervals were constructed for the observed quantile-level point estimates. Under the same assumptions as utilized in the central limit theorem for means, the sampling distribution for quantile values follows a normal distribution (Woodruff 1952) with expected value q_p, where p is the quantile probability of interest along the distribution (i.e., 0.01 or 0.95), and q is the quantile value at p. The variance is $\sigma^2_{q_p}/n$, where $\sigma_{q_p} = \sqrt{p(1-p)}/f_x(q_p)$ and $f_x(q_p)$ is the normal probability density function. Thus, for observed quantile value Q_n, a $100(1-\alpha)\%$ confidence interval for quantile value q_p at probability p is $Q_n \pm z_\alpha \sigma_{q_p}/\sqrt{n}$, where, n is the effective sample size of $R = 1000$.

The 95% confidence intervals ($\alpha = 0.05$) for the 0.01 quantile level of both *Aquarius* and Argo in the global region are (32.50, 32.98) and (33.00, 33.36), respectively. As the confidence intervals do not overlap, a significant difference between the 0.01 quantile levels of *Aquarius* and Argo is indicated. To conduct the test

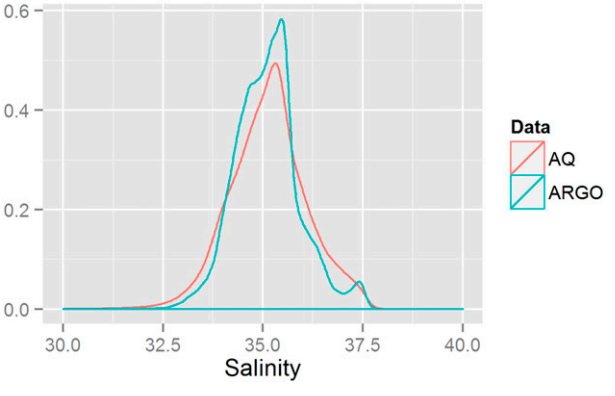

FIG. 1. Worldwide comparison of the pdfs for Argo and *Aquarius*.

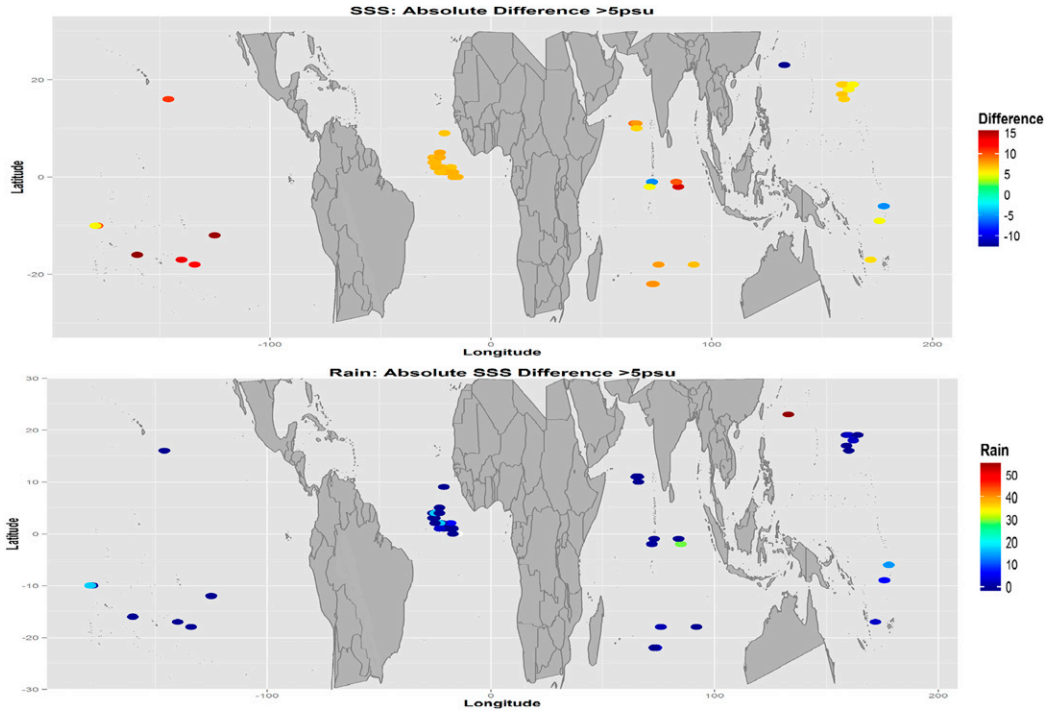

FIG. 2. (top) Absolute SSS difference greater than 5 psu for *Aquarius*–Argo and (bottom) corresponding rain (mm day^{-1}).

across multiple quantiles, a Bonferroni correction for multiple testing must be implemented. Thus, to test the 0.01, 0.05, and 0.10 quantile levels simultaneously, an effective α of 0.05/3 is utilized. This more conservative test indicates no significant difference between *Aquarius* and Argo at the 0.01 quantile level, but it does indicate significant differences at both the 0.05 and 0.10 quantile levels. No significant difference was observed globally at the higher quantile levels in the upper tail of the distribution.

The global quantile trends for the ascending and descending *Aquarius* tracks are in general agreement with each other and show the same pattern when compared to the Argo quantiles. The *Aquarius* ascending and descending paths are in general agreement with each other across averages and quantile levels. Thus, for the purposes of this analysis, a path comparison is not furthered considered.

The differences seen across the tails of the *Aquarius* and Argo distributions raises the question of an effect on measurements due to rain. There is literature building with regard to the rain effect on remotely sensed SSS versus in situ measurements, including Boutin et al. (2014). While not the focus of this manuscript, we briefly considered the relationship of rain with large differences (>5 psu) between *Aquarius* and Argo. Rain is measured in millimeters per day and is matched in time and space as described in section 2d. Figure 2 shows the locations where the absolute difference between *Aquarius* and Argo is greater than 5 psu (top) and the corresponding rain in millimeters per day (bottom). While there is not an absolute trend in the large differences between *Aquarius* and Argo measurements, smaller values are clustered around the equator at 0° longitude in the Atlantic. A cluster is seen in the northwest Pacific as well, with the highest values appear in the South Pacific. In the SSS plot, the lowest negative difference (*Aquarius* − Argo) in SSS (top right) corresponds to the highest rain amount (55 mm). Another high SSS difference in the Indian Ocean corresponds to a rain value of 29 mm. However, these large differences may have little to do with rainfall, being much more related to mesoscale stirring of the salinity field. This particular location would be subject to it because of the Amazon plume and tropical instability waves. Figure 7 in Boutin et al. (2014) shows a negative trend in the differences of SMOS–Argo with respect to rain. This is in agreement with Fig. 2 here, which shows that in general the high (positive) values of the differences are associated with less rain. It is important to note that a rain event may have occurred before a salinity measurement was taken, or vice versa. Measurements are matched within a day but not necessarily within a 24-h period. An empirical analysis of

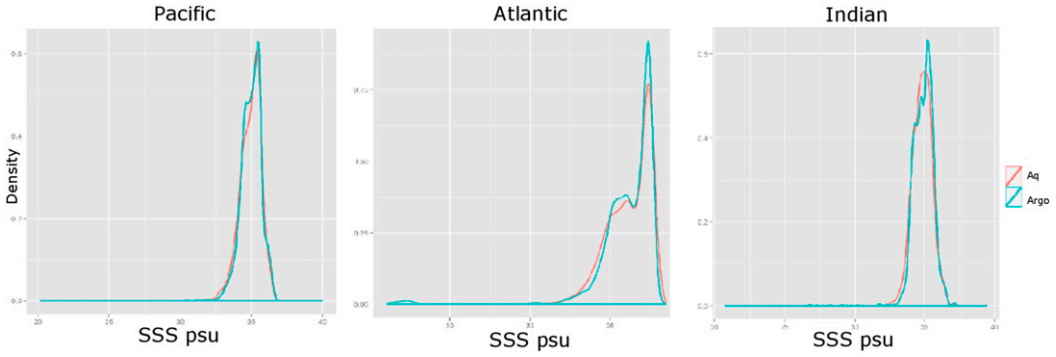

FIG. 3. Empirical probability distribution by ocean basin for Argo and *Aquarius*.

wind with respect to large SSS differences was also considered but no definitive relationship was seen. There was no apparent spatial relationship, and no changes in the magnitude of SSS difference with regard to the magnitude of the wind effect.

b. Regional ocean basin comparison

The empirical distribution of salinity for the two matched products for the Atlantic, Indian, and Pacific Oceans (Fig. 3) shows relative agreement within ocean basins while also indicating *Aquarius* more smoothly captures the distribution of salinity. However, there are subtle but important differences in the salinity distributions across ocean basins, particularly in the tails, as showcased in Fig. 3. For instance, in the Indian Ocean basin (right), the Argo distribution indicates essentially zero probability below 33, whereas the *Aquarius* distribution shows positive probability. Figure 3 shows bimodal peaks in the Atlantic Ocean basin at approximately 36.2 and 37.5, which are not shown in the *Aquarius* distribution. The Pacific Ocean exhibits slightly less variability, as indicated by the higher peak and tighter spread exhibited in the *Aquarius* density. Note also that the peaks of the Argo probability distribution functions are lower than those of *Aquarius* for all basins.

The means and standard deviations of the distributions of salinity for *Aquarius* and Argo within an ocean basin are compared in Table 2. The Atlantic Ocean exhibits significantly higher average salinity than both the Indian and Pacific Oceans, indicated by the nonoverlapping 95% confidence intervals. This is consistent across both the *Aquarius* and Argo products. It is interesting to note that the variation in *Aquarius* measurements is significantly more than that of Argo in the Pacific Ocean. This is denoted by the nonoverlapping (bold) confidence intervals for σ when comparing a variation within a salinity measurement source and across an ocean basin.

The empirical quantile distributions indicate that *Aquarius* has a longer lower tail than Argo across all ocean basins (Table 3). The lower-tail effect in *Aquarius* is particularly pronounced in the Indian and Pacific Oceans, where at the 0.01 and 0.05 quantile levels, the SSS values for *Aquarius* are on the order of 0.5 less than those of Argo.

The 95% confidence intervals ($\alpha = 0.05$) for the 0.01 quantile level of both *Aquarius* and Argo in all three ocean basins are considered. A significant difference is only observed in the Indian Ocean, with nonoverlapping intervals of (32.72, 33.14) and (33.36, 33.52), respectively, for the single test. Using a Bonferroni correction for multiple testing to compare the 0.01, 0.05, and 0.10 quantile levels simultaneously indicates significant differences in the observed quantile values for *Aquarius* and Argo at all three quantile levels tested. No significant difference was observed at the higher quantile levels in the upper tail of the distribution in any of the three ocean basins.

Examining the differences in SSS for *Aquarius*–Argo, 52.3% of the Atlantic differences are positive, with 48.3% of the Pacific differences positive and 38.1% in the Indian Ocean. For the large differences, 107 of the 110 absolute SSS differences greater than 5 psu are positive, including all 47 in the Atlantic.

c. Seasonal comparison by hemisphere

There is general agreement across seasons between *Aquarius* and Argo (Fig. 4), but the distributions exhibit some important distinctions. There are clear differences in seasonal patterns across the Northern and Southern Hemispheres across both *Aquarius* and Argo, such as a slightly lower mode of the salinity distribution and a longer upper tail in the Northern Hemisphere (Fig. 4. The higher and tighter peaks of the Argo distributions in spring and winter in both hemispheres (note the hemispheric seasonal definitions) may be due to the larger stratification of the upper ocean layer. A rain event is

TABLE 2. Salinity mean ($\bar{x}$) and standard deviation (s) by ocean basin: matched *Aquarius* and Argo. Significant difference between *Aquarius* and Argo at the $1 - \alpha = 0.95$ level is indicated in bold.

Ocean	Product	N	$\bar{x}$	95% CI for μ	s	95% CI for σ
Atlantic	*Aquarius*	3542	36.47	**(36.44, 36.49)**	0.803	(0.771, 0.843)
	Argo	3542	36.54	**(36.51, 36.56)**	0.755	(0.725, 0.793)
Indian	*Aquarius*	7648	34.70	**(34.69, 34.72)**	0.733	(0.703, 0.769)
	Argo	7648	34.90	**(34.89, 34.92)**	0.738	(0.708, 0.774)
Pacific	*Aquarius*	29 920	34.81	**(34.80, 34.82)**	0.806	**(0.774, 0.846)**
	Argo	29 920	34.98	**(34.97, 34.99)**	0.709	**(0.680, 0.744)**

more likely to mix in during winter and spring as the stratification effect is lessened.

Aquarius and Argo exhibit different central tendencies across each hemisphere and season, with nonoverlapping 95% confidence intervals in all cases (Table 4). Note that the standard deviations were obtained using the bootstrap method to account for the highly correlated measurements, as explained in section 3a. For each season, the average salinity in the Northern Hemisphere is consistently lower than in the Southern Hemisphere. For both products, the difference is statistically significant, indicated by the nonoverlapping 95% confidence bounds across both hemispheres for mean salinity. Table 4 also shows that the variation in the Southern Hemisphere is lower than in the Northern Hemisphere for all four seasons. This is indicated by the significantly smaller values for the standard deviation—the 95% confidence intervals for σ are nonoverlapping across both hemispheres for both products. The standard deviations are typically larger for *Aquarius* for all seasons across both hemispheres with the exception of winter in the Southern Hemisphere. The significantly different standard deviations across *Aquarius* and Argo (indicated in bold) yield nonoverlapping 95% confidence intervals for σ for spring and summer in each hemisphere, again indicating that *Aquarius* and Argo capture SSS variability differently in the Southern Hemisphere in the winter and spring seasons.

Examining the empirical quantile distribution in the Northern Hemisphere, *Aquarius* exhibits a longer tail (Table 5) with lower observed SSS at the lower quantile values, excepting the Northern winter season. The effect reverses in the Northern Hemisphere spring and summer in the upper half of the distribution in the higher quantiles, with *Aquarius* quantile values slightly higher than the corresponding Argo quantile values. This is illustrated in the cumulative distributions of Fig. 4. The same lower-tail relationship is seen in the Southern Hemisphere. The lower *Aquarius* quantile values are less than the corresponding Argo quantile values in the lower half of the distribution. This Southern Hemisphere trend continues in the upper half of the distribution, where the *Aquarius* quantile values are lower than the corresponding Argo quantile values.

The 95% confidence intervals for the 0.01 quantile level of both *Aquarius* and Argo across all seasons and both hemispheres are constructed. For the single test at one quantile level, a significant difference is observed in the Northern Hemisphere for the fall and spring seasons. This trend is maintained in the more conservative multiple comparison test across the lower three quantile levels—0.01, 0.05, and 0.10—for the fall and spring seasons. In the Southern Hemisphere, only the winter season does not indicate a significant difference in quantile values at the 0.01 quantile levels for *Aquarius* and Argo. Considering the multiple comparison test, both fall and summer are significant across the 0.01, 0.05, and 0.10 quantile levels. Spring shows a significant difference for the 0.05 and 0.10 quantiles but not the lowest quantile level, 0.01. No significant difference was observed at the higher quantiles levels in the upper tails of the distributions.

TABLE 3. Argo and *Aquarius* quantiles by ocean basin for all observations and observations matched in space and time.

Ocean	Product	N	0.01	0.05	0.10	0.25	0.50	0.75	0.90	0.95	0.99
Atlantic	*Aquarius*	3542	34.28	34.99	35.41	35.97	36.52	37.14	37.46	37.57	37.74
	Argo	3542	34.37	35.24	35.64	36.08	36.58	37.17	37.44	37.51	37.63
Indian	*Aquarius*	7648	32.93	33.52	33.76	34.17	34.74	35.22	35.61	35.86	36.20
	Argo	7648	33.44	33.92	34.09	34.43	34.96	35.37	35.67	35.90	36.40
Pacific	*Aquarius*	29 920	32.65	33.41	33.77	34.29	34.92	35.39	35.74	35.98	36.35
	Argo	29 920	33.13	33.78	34.09	34.52	35.04	35.48	35.79	36.09	36.44

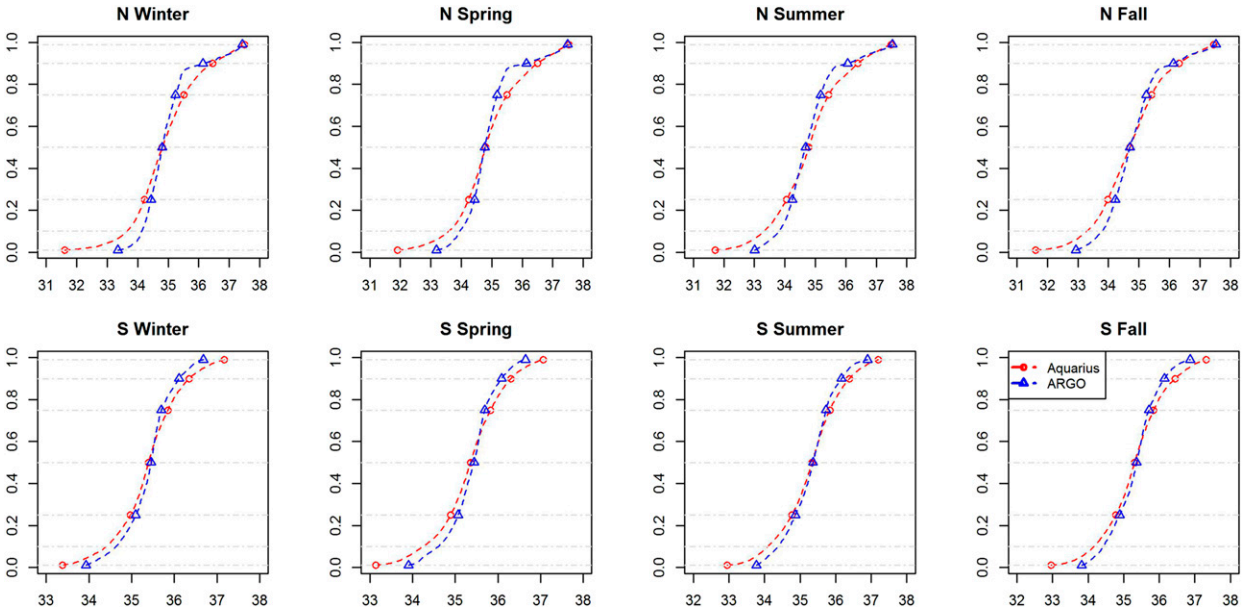

FIG. 4. Empirical cumulative distributions: Argo vs *Aquarius* for the four seasons across the (top) Northern and (bottom) Southern Hemispheres.

4. Temporal and spatial behavior

Dependence, patterns over time, seasonal trends, and tail behavior are all indicative of salinity's interaction with the global water cycle. They can also lead to important understandings about salinity's relationship with surface-level meteorological factors and synoptic weather events. We examine how *Aquarius* and Argo compare across these characteristics.

Temporal trends

Certain regions are of specific interest because they exhibit interesting and possibly unique characteristics due to physical properties of the region. We divide the area of study into eight regions in order to consider a more focused comparison (Fig. 5).

Figure 6 compares the empirical probability densities of the *Aquarius* and Argo products across the eight

TABLE 4. Variables $\bar{x}$ and s by season and hemisphere: *Aquarius* and Argo. Northern Hemisphere: winter (summer) is represented by January–March (July–September). Southern Hemisphere: summer (winter) is represented by January–March (July–September). Significant difference between *Aquarius* and Argo at the $1-\alpha=0.95$ level is indicated in bold.

Hemisphere	Season	Product	N	$\bar{x}$	95% CI for μ	s	95% CI for σ
North	Fall	*Aquarius*	5983	34.60	**(34.57, 34.62)**	1.03	(0.99, 1.08)
		Argo	5983	34.81	**(34.79, 34.84)**	0.94	(0.91, 0.99)
	Winter	*Aquarius*	3910	34.82	**(34.79, 34.85)**	0.96	(0.92, 1.00)
		Argo	3910	34.92	**(34.89, 34.95)**	0.88	(0.85, 0.93)
	Spring	*Aquarius*	5491	34.73	**(34.70, 34.76)**	1.03	**(0.99, 1.08)**
		Argo	5491	34.89	**(34.86, 34.91)**	0.91	**(0.87, 0.95)**
	Summer	*Aquarius*	4982	34.61	**(34.58, 34.64)**	1.07	**(1.03, 1.12)**
		Argo	4982	34.80	**(34.77, 34.82)**	0.95	**(0.91, 1.00)**
South	Fall	*Aquarius*	5188	35.15	**(35.13, 35.17)**	0.74	(0.71, 0.78)
		Argo	5188	35.30	**(35.28, 35.32)**	0.68	(0.65, 0.72)
	Winter	*Aquarius*	4898	35.26	**(35.24, 35.28)**	0.66	(0.64, 0.70)
		Argo	4898	35.37	**(35.35, 35.39)**	0.70	(0.68, 0.74)
	Spring	*Aquarius*	6796	35.19	**(35.18, 35.21)**	0.70	**(0.67, 0.73)**
		Argo	6796	35.38	**(35.37, 35.39)**	0.61	**(0.59, 0.64)**
	Summer	*Aquarius*	3898	35.14	**(35.11, 35.16)**	0.78	**(0.75, 0.82)**
		Argo	3898	35.31	**(35.28, 35.33)**	0.71	**(0.68, 0.74)**

TABLE 5. Argo and *Aquarius* quantile by season and hemisphere for matched observations.

Hemisphere	Season	SSS	0.01	0.05	0.1	0.25	0.5	0.75	0.9	0.95	0.99
North	Fall	*Aquarius*	32.54	33.11	33.45	33.93	34.47	35.18	35.89	36.71	37.47
		Argo	32.83	33.40	33.74	34.23	34.68	35.24	36.14	36.86	37.53
	Winter	*Aquarius*	32.89	33.66	33.90	34.26	34.66	35.24	35.94	37.01	37.57
		Argo	32.37	33.84	34.12	34.40	34.77	35.24	36.09	36.99	37.45
	Spring	*Aquarius*	32.47	33.26	33.61	34.14	34.63	35.15	36.02	37.11	37.63
		Argo	33.01	33.69	33.96	34.42	34.77	35.19	36.17	37.07	37.48
	Summer	*Aquarius*	32.53	33.09	33.44	33.94	34.50	35.15	35.96	36.95	37.52
		Argo	32.75	33.35	33.75	34.22	34.67	35.19	36.15	36.99	37.55
South	Fall	*Aquarius*	33.30	33.88	34.18	34.67	35.20	35.62	36.05	36.30	36.91
		Argo	33.79	34.16	34.43	34.85	35.34	35.67	36.16	36.40	36.92
	Winter	*Aquarius*	33.53	34.03	34.41	34.90	35.32	35.65	36.08	36.28	36.72
		Argo	33.79	34.23	34.61	35.08	35.45	35.68	36.10	36.35	36.77
	Spring	*Aquarius*	33.34	33.89	34.22	34.83	35.28	35.63	36.01	36.22	36.61
		Argo	33.87	34.24	34.60	35.07	35.45	35.70	36.11	36.32	36.65
	Summer	*Aquarius*	33.20	33.79	34.08	34.65	35.21	35.64	36.06	36.32	36.88
		Argo	33.77	34.11	34.38	34.83	35.36	35.73	36.20	36.40	36.93

defined ocean regions. The Argo empirical distribution tends to have higher and tighter peaks in both hemispheres, with *Aquarius* capturing the lower tail of SSS more completely in the Southern Hemisphere. This is particularly noticeable in the northwest Pacific and North Atlantic regions, and southwest Pacific and south Atlantic regions, respectively. The north Indian basin is an exception, probably because of its small extent and extreme seasonality (Rao and Sivakumar 2003).

Figure 7 displays the time series of vertical box plots of the distribution of salinity by date for the eight regions. The upper and lower bounds of the vertical boxes in the plots represent the first and third quartiles, respectively, of the salinity distribution at each date. Thus, the dark shaded areas represent the bulk of the distribution. Values beyond 1.5 times the interquartile range (IQR) are seen as dots above and mainly below these dark areas. The box plots for the *Aquarius* product (Fig. 7, right) capture more variability than the Argo version, especially in the Northern Hemisphere. There are seasonal changes in the distributional characteristics of SSS in the lower tails, while the upper parts of the distributions, as well as the medians, remain relatively constant for all basins (Fig. 7, right column). Each basin has its own distinct seasonality. In the North Pacific [northeast Pacific (NEP) and northwest Pacific (NWP)], the distributions get wider in the fall but are tighter and have more values in the tails in the spring. The south Indian basin is similar in pattern to the northwest Pacific. In the south Atlantic and southeast Pacific, there tends to be a lot of low-lying values in the winter and early spring. The north Indian basin shows a slight increase in the number of lower-tail values in the winter. In the North Atlantic, there is less seasonality exhibited, but there is an increase in the number of low SSS values in the summer. Note that the maxima and upper tails of the SSS distribution over time stay fairly consistent, whereas a seasonal trend can be seen in the lower tails (minima) around November–February of each year, with a few

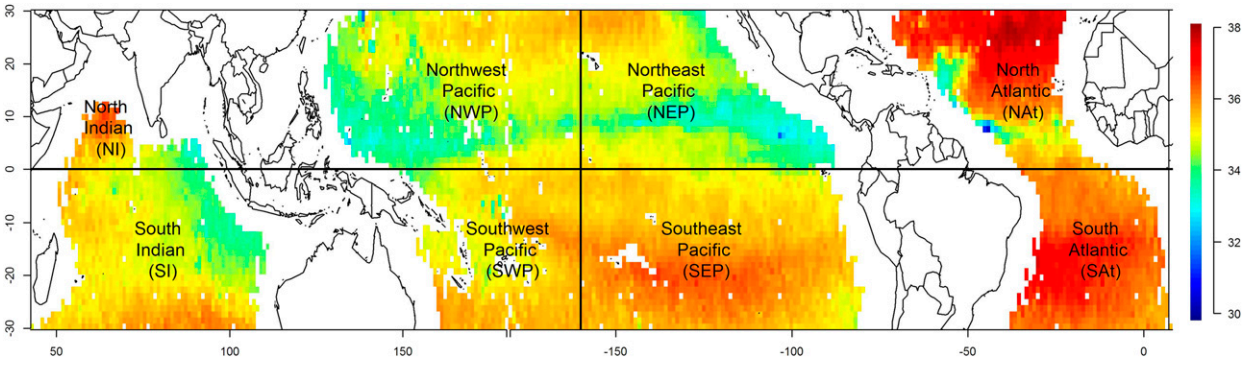

FIG. 5. *Aquarius* SSS for the week of 26 Aug 2011–2 Sep 2011 across the eight defined regions.

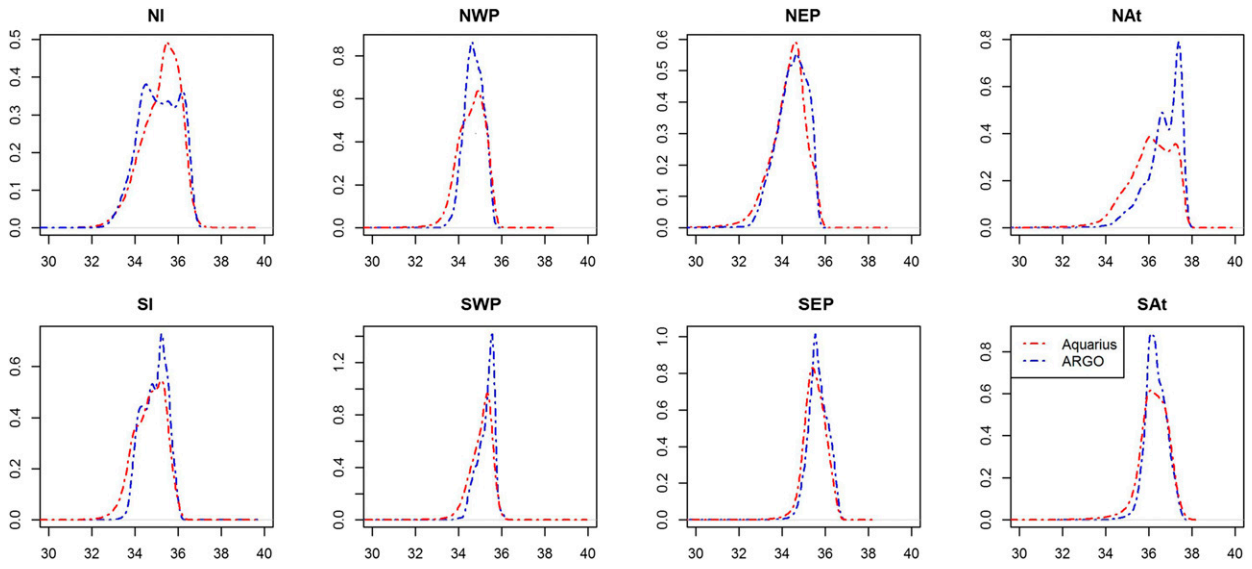

FIG. 6. Empirical densities: Argo vs *Aquarius* for the eight regions displayed in Fig. 5.

extremes in the summer and fall months in 2011 and 2012. However, the minima shows seasonal effects particularly in the North Pacific and southeast Pacific winter months, with smaller magnitude seen in winter and spring in the Atlantic.

The box plot time series for the Argo product (Fig. 7, left column) largely displays little of the seasonality exhibited in *Aquarius*, with the exception of slight winter trends shown in the Pacific regions. In all regions, *Aquarius* captures more variability—especially in the Northern Hemisphere.

5. Comparing SPURS regions

Given the possible dependence of the SSS distribution on rainfall, we compare distributions in two regions associated with SSS field campaigns: the sites of SPURS-1 in the subtropical North Atlantic (15°–30°N, 30°–45°W; Lindstrom et al. 2015) and SPURS-2 in the tropical eastern Pacific (0°–10°N, 120°–130°W; Schmitt et al. 2015). These sites represent evaporation-dominated and rainfall-dominated areas, respectively. SPURS-1 was carried out in 2012/13 and SPURS-2 is anticipated to take place in 2016/17. The SPURS-1 region is one of high SSS, relatively low variability, weak seasonality, and stable forcing (Bingham et al. 2014; D'Addezio and Bingham 2014). The SPURS-2 region has lower SSS and very strong seasonality in both SSS (Bingham et al. 2012; Bingham et al. 2010) and rainfall (Waliser and Gauthier, 1993).

Table 6 compares the means and standard deviations for the two SPURS regions, calculated as in section 3a using a bootstrap sample of $R = 200$ to account for the smaller N. In both regions, *Aquarius*'s mean SSS is below that of Argo's, although the difference is only significant in the SPURS-2 region. The increased trend in *Aquarius*'s variation over Argo previously observed is exhibited as well, and the standard deviations are significantly different across the SPURS-1 region.

Figure 8 displays the times series of vertical box plots of the distribution of salinity by date for the SPURS regions. The results show *Aquarius* capturing more of the tails of the distribution, especially in the lower tails. Seasonal trends are more pronounced in the *Aquarius* box plots for both regions, particularly in the SPURS-2 regions where *Aquarius* captures more low-lying SSS values.

The empirical cumulative distributions by season (Fig. 9; Table 7) indicate much stronger agreement between Argo and *Aquarius* in the SPURS-2 region than SPURS-1. In both regions the lower tail is fatter for the *Aquarius* data as we have found in previous sections, especially at the 0.10 quantile. However, in the SPURS-1 region, this difference extends well up to about the 0.75 quantile. In the SPURS-2 region, the distributions agree reasonably well at the center, with the exception of the summer. This result is different from what might be expected if the lower tails of the distributions are driven entirely by rainfall. This seems to suggest that *Aquarius*'s heavier lower tail is a result of not only very shallow surface rain puddles but also of the presence or absence of winds to mix those puddles rapidly down into the bulk mixed layer. The SPURS-1 region is not without rainfall, especially in the fall

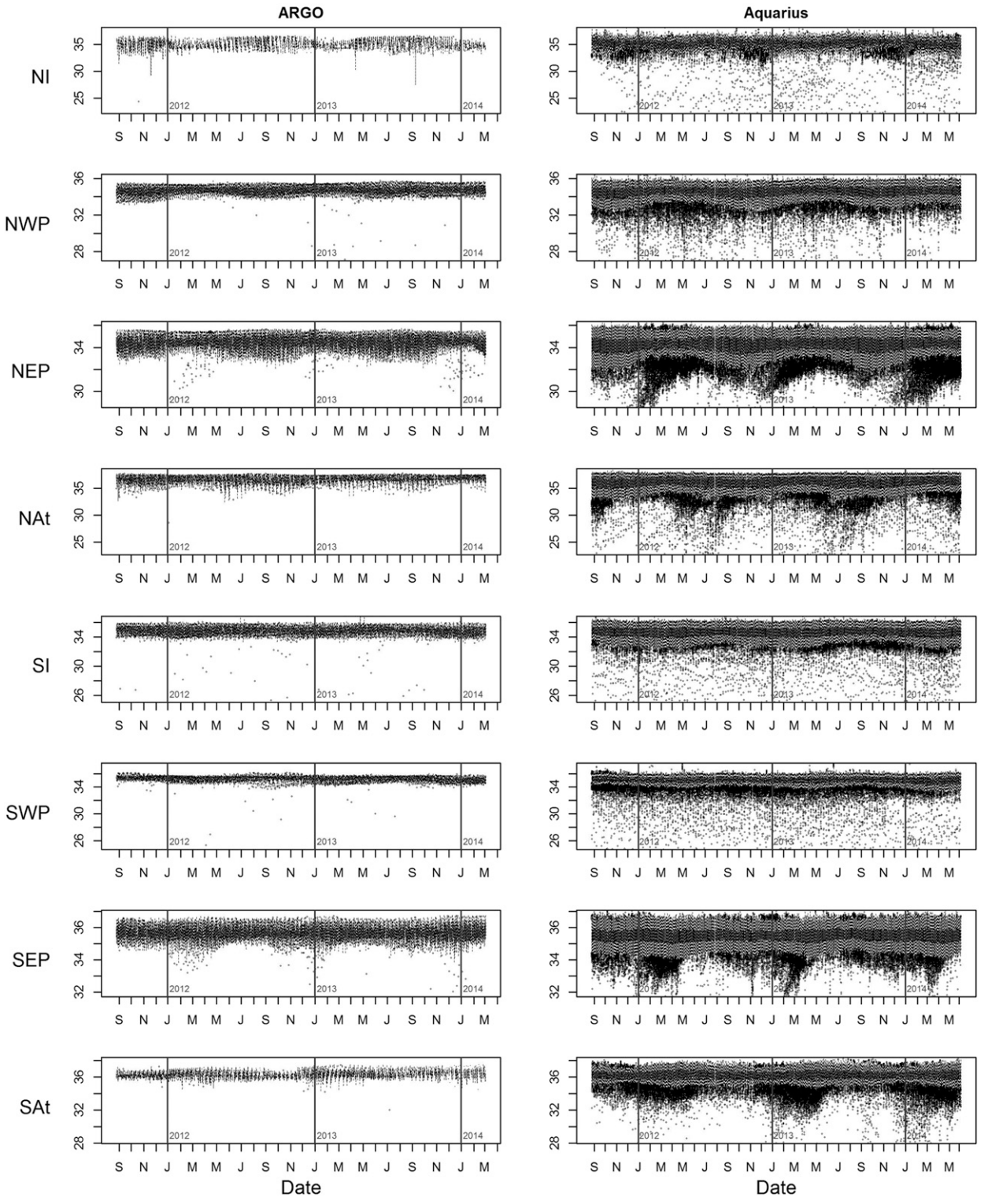

FIG. 7. Salinity distribution over time for the eight regions: (left) Argo and (right) *Aquarius*. Note that the psu scales (vertical axis) are different across spatial regions but are identical within regions to enable comparison between *Aquarius* and Argo. The upper and lower bounds of the vertical boxes in the plots represent the first and third quartiles, respectively, of the salinity distribution at each date. Values beyond 1.5 times the IQR are shown as dots.

TABLE 6. Variables $\bar{x}$ and s by SPURS region: *Aquarius* and Argo. Significant difference between *Aquarius* and Argo at the $1 - \alpha = 0.95$ level is indicated in bold. Effective sample size used in bootstrapping for s is $r = 200$.

SPURS	Product	N	$\bar{x}$	95% CI for μ	s	95% CI for σ
1	*Aquarius*	682	37.25	(37.23, 37.38)	0.381	**(0.347, 0.422)**
	Argo	411	37.27	(37.26, 37.29)	0.297	**(0.270, 0.329)**
2	*Aquarius*	682	34.08	**(34.05, 34.11)**	0.512	(0.466, 0.568)
	Argo	411	34.29	**(34.25, 34.31)**	0.441	(0.401, 0.489)

(D'Addezio and Bingham 2014), but the SPURS-2 region is much windier than SPURS-1.

6. Discussion

Throughout this paper it has consistently been seen that the probability distribution of *Aquarius* has longer, thicker tails and shorter central peaks than Argo (Figs. 1, 3, and 6). The longer tails are especially apparent in the lower portion of the distribution (Fig. 6). As stated above, this could be either due to the lower accuracy of *Aquarius* or the better ability of *Aquarius* to capture tail events. The second explanation seems more likely and plausible, however, as evidenced by the box plots of Fig. 7. This is a good sign for the future use of *Aquarius* data. While Argo can tell us about the mean SSS, *Aquarius* gives us much more information about the variability. As this variability is the result of events that may modify SSS, such as rainfall, evaporation, horizontal mixing, and upwelling, *Aquarius* can tell us where and when these processes are occurring: that is, *Aquarius* can actually begin to fulfill its mission as an ocean rain gauge (Lagerloef et al. 2008; Grunseich et al. 2013).

All of this assumes that *Aquarius* is accurately measuring values at the tails of the distribution. There are two retrieval issues that could cause an enhancement of lower-tail values: RFI and land contamination. We screened out land values higher than 0.5% so that should not be an issue. Also, we would not see the clear seasonality in Fig. 7 if low values were caused by land contamination. Though RFI is an issue, the lower values are present in both the SPURS-1 and SPURS-2 results. Both of these areas are far from known sources of RFI (Lagerloef et al. 2013). The *Aquarius* retrieval algorithm is also known to be sensitive to sea state and rain rate (Lagerloef et al. 2008). Tang et al. (2014b) in comparing the rain-corrected CAP version of the *Aquarius* data with the HYCOM model found there was little systematic difference between *Aquarius* and HYCOM as a function of rain rate or wind speed (see Fig. 4b in Tang et al. 2014b). We assume similar behavior from the non-CAP, rain-corrected version of *Aquarius* used in this paper. The results of this paper emphasize the need for an alternative validation dataset that measures the near-skin-surface SSS under calm conditions.

Assuming there are no issues with the retrieval algorithm, the clear result of this paper is that *Aquarius* captures tail variability in a way not previously seen. Another way of saying this is that tail variability is large and important enough to have an impact on the

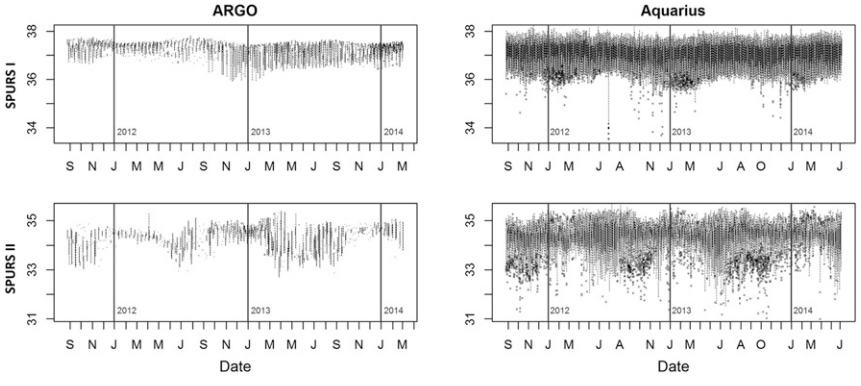

FIG. 8. Salinity distribution over time for the SPURS regions: (left) Argo and (right) *Aquarius*. Note that the psu scales (vertical axis) are as in Fig. 7. The upper and lower bounds of the vertical boxes in the plots represent the first and third quartiles, respectively, of the salinity distribution at each date. Values beyond 1.5 times the IQR are shown as dots.

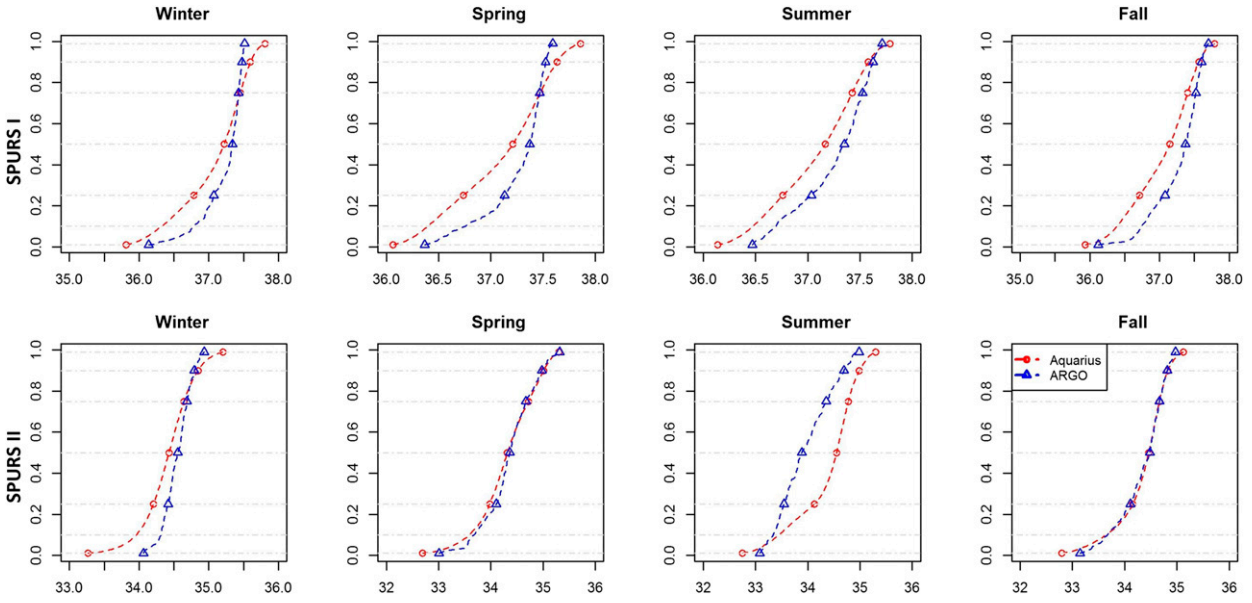

FIG. 9. Empirical cumulative distributions: (top) SPURS-1 and (bottom) SPURS-2 regions.

SSS field at the scale of the *Aquarius* footprint. Low-salinity events, regardless of their nature or how they originated, can affect the average SSS over a larger area. These events are not captured well by the Argo array. The most likely explanation is that such events are strongly confined to the near-surface, above the sampling depth of standard Argo floats (Asher et al. 2014b; Boutin et al. 2014; Tang et al. 2014b; Henocq et al. 2010). However, the relationship between rainfall and low-salinity outliers is not simple, as illustrated by the comparison between the SPURS-1 and -2 regions. To fulfill the *Aquarius* mission as an ocean rain gauge, we will need to use the lower tail of the SSS distribution, but with an understanding of the spatial scale of low-salinity events and how they may be related to wind and evaporation (Meissner et al. 2014b). Using the lower tail, we may be able to separate the effects of ocean dynamics from local meteorology.

A real understanding of the probability distribution of SSS, the space and time scales of its variations, and its connection to processes like surface forcing, ocean mixing, and stirring, and upwelling/downwelling, awaits future researchers. Characteristics such as those depicted in Figs. 8 and 9 are a beginning to that process. What seems most evident from the results of this paper, though, is that the key to this connection

TABLE 7. SPURS regions by seasons.

SPURS	Season	Product	*N*	0.05	0.10	0.25	0.50	0.75	0.90	0.95
1	Fall	*Aquarius*	170	36.36	36.68	36.98	37.27	37.47	37.61	37.68
		Argo	170	36.67	36.78	37.10	37.40	37.53	37.60	37.63
	Winter	*Aquarius*	132	36.53	36.80	37.19	37.42	37.57	37.69	37.76
		Argo	132	36.74	36.84	37.04	37.34	37.43	37.48	37.50
	Spring	*Aquarius*	224	36.56	36.64	37.07	37.38	37.56	37.70	37.77
		Argo	224	36.63	36.91	37.13	37.36	37.45	37.52	37.54
	Summer	*Aquarius*	156	36.61	36.70	37.09	37.32	37.50	37.62	37.64
		Argo	156	36.65	36.85	37.17	37.39	37.56	37.64	37.69
2	Fall	*Aquarius*	122	33.20	33.38	33.78	34.07	34.33	34.50	34.63
		Argo	122	33.42	33.87	34.13	34.41	34.57	34.72	34.77
	Winter	*Aquarius*	68	33.94	34.13	34.30	34.42	34.60	34.72	34.90
		Argo	68	34.25	34.32	34.43	34.58	34.69	34.75	34.79
	Spring	*Aquarius*	115	33.44	33.71	33.92	34.17	34.51	34.85	35.01
		Argo	115	33.81	33.99	34.16	34.39	34.61	34.94	35.03
	Summer	*Aquarius*	106	32.83	33.00	33.35	33.74	34.34	34.60	34.69
		Argo	106	33.24	33.40	33.56	33.98	34.33	34.68	34.88

lies in the tails of the distribution, especially the lower tail. The low-probability events that the *Aquarius* satellite is able to capture shine a light on the events that define the hydrologic cycle and the global transport of freshwater that will play a crucial role in the future of a warming planet.

Acknowledgments. Elizabeth Mannshardt was supported as a postdoctoral research scholar through the National Science Foundation's Collaborative Research: RNMS Statistical Methods for Atmospheric and Oceanic Sciences under Grant DMS-1107046. Frederick Bingham and Katarina Sucic were funded by NASA under Grants NNX09AU70G and NNX11AE83G. We thank two anonymous reviewers for their constructive comments, which helped improve the manuscript.

REFERENCES

Abe, H., and N. Ebuchi, 2014: Evaluation of sea-surface salinity observed by Aquarius. *J. Geophys. Res. Oceans*, **119**, 8109–8121, doi:10.1002/2014JC010094.

Alory, G., C. Maes, T. Delcroix, N. Reul, and S. Illig, 2012: Seasonal dynamics of sea surface salinity off Panama: The far eastern Pacific fresh pool. *J. Geophys. Res.*, **117**, C04028, doi:10.1029/2011JC007802.

Argo, 2000: Argo float data and metadata from Global Data Assembly Centre (Argo GDAC). Ifremer, accessed 14 December 2015, doi:10.12770/1282383d-9b35-4eaa-a9d6-4b0c24c0cfc9.

Asher, W. E., A. T. Jessup, R. Branch, and D. Clark, 2014a: Observations of rain-induced near-surface salinity anomalies. *J. Geophys. Res. Oceans*, **119**, 5483–5500, doi:10.1002/2014JC009954.

——, ——, and D. Clark, 2014b: Stable near-surface ocean salinity stratifications due to evaporation observed during STRASSE. *J. Geophys. Res. Oceans*, **119**, 3219–3233, doi:10.1002/2014JC009808.

Bingham, F. M., S. D. Howden, and C. J. Koblinsky, 2002: Sea surface salinity measurements in the historical database. *J. Geophys. Res.*, **107**, 8019, doi:10.1029/2000JC000767.

——, G. R. Foltz, and M. J. McPhaden, 2010: Seasonal cycles of surface layer salinity in the Pacific Ocean. *Ocean Sci.*, **6**, 775–787, doi:10.5194/os-6-775-2010.

——, ——, and ——, 2012: Characteristics of the seasonal cycle of surface layer salinity in the global ocean. *Ocean Sci.*, **8**, 915–929, doi:10.5194/os-8-915-2012.

——, J. Busecke, A. L. Gordon, C. Giulivi, and Z. Li, 2014: The North Atlantic subtropical surface salinity maximum as observed by Aquarius. *J. Geophys. Res. Oceans*, **119**, 7741–7755, doi:10.1002/2014JC009825.

Boutin, J., N. Martin, G. Reverdin, X. Yin, and F. Gaillard, 2013: Sea surface freshening inferred from SMOS and ARGO salinity: Impact of rain. *Ocean Sci.*, **9**, 183–192, doi:10.5194/os-9-183-2013.

——, ——, ——, S. Morisset, X. Yin, L. Centurioni, and N. Reul, 2014: Sea surface salinity under rain cells: SMOS satellite and in situ drifters observations. *J. Geophys. Res. Oceans*, **119**, 5533–5545, doi:10.1002/2014JC010070.

Busecke, J., A. L. Gordon, Z. Li, F. M. Bingham, and J. Font, 2014: Subtropical surface layer salinity budget and the role of mesoscale turbulence. *J. Geophys. Res. Oceans*, **119**, 4124–4140, doi:10.1002/2013JC009715.

D'Addezio, J. M., and F. M. Bingham, 2014: A subtropical North Atlantic regional atmospheric moisture budget. *J. Geophys. Res. Oceans*, **119**, 8731–8748, doi:10.1002/2014JC01030.

Drucker, R., and S. C. Riser, 2014: Validation of Aquarius sea surface salinity with Argo: Analysis of error due to depth of measurement and vertical salinity stratification. *J. Geophys. Res. Oceans*, **119**, 4626–4637, doi:10.1002/2014JC010045.

Efron, B., and R. Tibshirani, 1986: Bootstrap methods for standard errors, confidence intervals, and other measures of statistical accuracy. *Stat. Sci.*, **1**, 54–75, doi:10.1214/ss/1177013815.

Foltz, G. R., and M. J. McPhaden, 2008: Seasonal mixed layer salinity balance of the tropical North Atlantic Ocean. *J. Geophys. Res.*, **113**, C02013, doi:10.01029/02007JC004178.

Grunseich, G., B. Subrahmanyam, and B. Wang, 2013: The Madden-Julian oscillation detected in Aquarius salinity observations. *Geophys. Res. Lett.*, **40**, 5461–5466, doi:10.1002/2013GL058173.

Hasson, T., A. Delcroix, J. Boutin, R. Dussin, and J. Ballabrera-Poy, 2014: Analyzing the 2010–2011 La Niña signature in the tropical Pacific sea surface salinity using in situ data, SMOS observations, and a numerical simulation. *J. Geophys. Res. Oceans*, **119**, 3855–3867, doi:10.1002/2013JC009388.

Henocq, C., J. Boutin, G. Reverdin, F. Petitcolin, S. Arnault, and P. Lattes, 2010: Vertical variability of near-surface salinity in the tropics: Consequences for L-band radiometer calibration and validation. *J. Atmos. Oceanic Technol.*, **27**, 192–209, doi:10.1175/2009JTECHO670.1.

Hodges, B. A., and D. M. Fratantoni, 2014: AUV observations of the diurnal surface layer in the North Atlantic salinity maximum. *J. Phys. Oceanogr.*, **44**, 1595–1604, doi:10.1175/JPO-D-13-0140.1.

Klein, L. A., and C. Swift, 1977: An improved model for the dielectric constant of sea water at microwave frequencies. *IEEE Trans. Antennas Propag.*, **25**, 104–111, doi:10.1109/TAP.1977.1141539.

Lagerloef, G., and Coauthors, 2008: The Aquarius/SAC-D mission: Designed to meet the salinity remote-sensing challenge. *Oceanography*, **21** (1), 68–81, doi:10.5670/oceanog.2008.68.

——, and Coauthors, 2013: Aquarius salinity validation analysis: Data version 2.0. Aquarius Project Doc. AQ-014-PS-0016, 36 pp.

——, H.-Y. Kao, T. Meissner, and J. Vazquez, 2015: Aquarius salinity validation analysis; version 4.0. PODAAC, accessed 14 December 2015. [Available online at ftp://podaac-ftp.jpl.nasa.gov/allData/aquarius/docs/v4/AQ-014-PS-0016_AquariusSalinityDataValidationAnalysis_DatasetVersion4.0and3.0.pdf.]

Lee, T., G. Lagerloef, M. M. Gierach, H.-Y. Kao, S. Yueh, and K. K. Dohan, 2012: Aquarius reveals salinity structure of tropical instability waves. *Geophys. Res. Lett.*, **39**, L12610, doi:10.1029/2012GL052232.

Le Vine, D. M., G. Lagerloef, F. Colomb, S. Yueh, and F. Pellerano, 2007: Aquarius: An instrument to monitor sea surface salinity from space. *IEEE Trans. Geosci. Remote Sens.*, **45**, 2040–2050, doi:10.1109/TGRS.2007.898092.

Lindstrom, E., F. Bryan, and R. Schmitt, 2015: Salinity Processes in the Upper-ocean Regional Study—The North Atlantic Experiment. *Oceanography*, **28** (1), 14–19, doi:10.5670/oceanog.2015.01.

Meissner, T., F. Wentz, and L. Ricciardulli, 2014a: The emission and scattering of L-band microwave radiation from rough ocean surfaces and wind speed measurements from the Aquarius sensor. *J. Geophys. Res. Oceans*, **119**, 6499–6522, doi:10.1002/2014JC009837.

——, ——, J. Scott, and K. Hilburn, 2014b: Assessment of rain impact on the Aquarius salinity retrievals. University of Washington. [Available online at http://depts.washington.edu/uwconf/aquarius_sacd/meissner_rain_effects.pptx.]

NASA, 2012: Aquarius: Sea surface salinity from space. [Available online at http://aquarius.nasa.gov/index.html.]

OBPG, 2014: Aquarius official release level 2 sea surface salinity & wind speed data V3.0. NASA PODAAC, accessed 14 December 2015, doi:10.5067/AQUAR-2S1PS.

PO.DAAC, 2014: *Aquarius* user guide: *Aquarius* dataset version 3.0. PODAAC, accessed 10 December 2015. [Available online at ftp://podaac-ftp.jpl.nasa.gov/SalinityDensity/aquarius/docs/v3/AQ-010-UG-0008_AquariusUserGuide_DatasetV3.0.pdf.]

Qu, T., S. Gao, and I. Fukumori, 2011: What governs the North Atlantic salinity maximum in a global GCM? *Geophys. Res. Lett.*, **38**, L07602, doi:10.1029/2011GL046757.

Rao, R. R., and R. Sivakumar, 2003: Seasonal variability of sea surface salinity and salt budget of the mixed layer of the north Indian Ocean. *J. Geophys. Res.*, **108**, 3009, doi:10.1029/2001JC000907.

Santos-Garcia, A., M. M. Jacob, W. L. Jones, W. E. Asher, Y. Hejazin, H. Ebrahimi, and M. Rabolil, 2014: Investigation of rain effects on Aquarius sea surface salinity measurements. *J. Geophys. Res. Oceans*, **119**, 7605–7624, doi:10.1002/2014JC010137.

Schmitt, R. W., and Coauthors, 2015: From salty to fresh salinity processes in the upper-ocean regional study-2 (SPURS-2): Diagnosing the physics of a rainfall-dominated salinity minimum. *Oceanography*, **28** (1), 150–159, doi:10.5670/oceanog.2015.15.

Sheskin, D., 2011: *Handbook of Parametric and Nonparametric Statistical Procedures*. 5th ed. Chapman and Hall/CRC, 1926 pp.

Tang, W., S. H. Yueh, A. Fore, G. Neumann, A. Hayashi, and G. Lagerloef, 2013: The rain effect on Aquarius' L-band sea surface brightness temperature and radar backscatter. *Remote Sens. Environ.*, **137**, 147–157, doi:10.1016/j.rse.2013.06.016.

——, ——, A. G. Fore, and A. Hayashi, 2014a: Validation of Aquarius sea surface salinity with in situ measurements from Argo floats and moored buoys. *J. Geophys. Res. Oceans*, **119**, 6171–6189, doi:10.1002/2014JC010101.

——, ——, ——, ——, T. Lee, and G. Lagerloef, 2014b: Uncertainty of Aquarius sea surface salinity retrieved under rainy conditions and its implication on the water cycle study. *J. Geophys. Res. Oceans*, **119**, 4821–4839, doi:10.1002/2014JC009834.

Vinogradova, N. T., and R. M. Ponte, 2013: Clarifying the link between surface salinity and freshwater fluxes on monthly to interannual time scales. *J. Geophys. Res. Oceans*, **118**, 3190–3201, doi:10.1002/jgrc.20200.

Waliser, D. E., and C. Gauthier, 1993: A satellite-derived climatology of the ITCZ. *J. Climate*, **6**, 2162–2174, doi:10.1175/1520-0442(1993)006<2162:ASDCOT>2.0.CO;2.

Woodruff, R. S., 1952: Confidence intervals for medians and other position measure. *J. Amer. Stat. Assoc.*, **47**, 635–646, doi:10.1080/01621459.1952.10483443.

Yu, L., 2010: On sea surface salinity skin effect induced by evaporation and implications for remote sensing of ocean salinity. *J. Phys. Oceanogr.*, **40**, 85–102, doi:10.1175/2009JPO4168.1.

——, 2011: A global relationship between the ocean water cycle and near-surface salinity. *J. Geophys. Res.*, **116**, C10025, doi:10.1029/2010JC006937.

——, 2014: Coherent evidence from Aquarius and Argo for the existence of a shallow low-salinity convergence zone beneath the Pacific ITCZ. *J. Geophys. Res. Oceans*, **119**, 7625–7644, doi:10.1002/2014JC010030.

Yueh, S., and J. Chaubell, 2012: Sea surface salinity and wind retrieval using combined passive and active L-band microwave observations. *IEEE Trans. Geosci. Remote Sens.*, **50**, 1022–1032, doi:10.1109/TGRS.2011.2165075.